Robust Resiliency-Oriented Operation of Active Distribution Networks Considering Windstorms

Moein Esfahani, Nima Amjady, *Senior Member, IEEE*, Bahareh Bagheri, and Nikos D. Hatziargyriou, *Fellow, IEEE*

***Abstract*—Recent climate changes have created intense natural disasters, such as windstorms, which can cause significant damages to power grids. System resilience is defined as the ability of the system to withstand such high-impact low-probability events. This paper proposes a robust resilient operational schedule for active distribution networks against windstorms. In order to capture dynamic behaviors of these disasters, zonal disaster-specific uncertainty sets associated with the windstorm are proposed. Additionally, the unavailability uncertainties of *N-K* contingencies as well as the forecast uncertainties of load demand, wind power, and solar power are taken into account. Instead of committing microturbines and energy storage systems in the first stage (*here-and-now*) of the decision-making process, the proposed model considers these commitment decisions in the second stage (*wait-and-see*) of the decision-making process, which is more consistent with the fast response time of these units. Since the second stage of the proposed model has binary decision variables, recent KKT-based and duality-based methods are not applicable. Therefore, a new solution method based on block coordinate descent (BCD) and line search (LS) techniques is proposed to solve the bi-level problem. Eventually, IEEE 33-bus distribution test system is used to illustrate the effectiveness of the proposed model and solution method.**

***Index Terms*—Active distribution network, block coordinate descent, robust resiliency-oriented operation, windstorm.**

NOMENCLATURE

Indices and Symbols

i, j	Indices of buses.
k	Index of zones.
t	Index of time periods.
n	Index of linearization model of $\cos(\theta_i - \theta_j)$.
$^{\max}$, $^{\min}$	Superscripts indicating maximum and minimum limits.
γ, λ, ν	Superscripts indicating iteration γ of LS outer loop, iteration λ of LS inner loop, and iteration v of BCD loop, respectively.

Sets:

T	Set of time periods (t_1 to t_s.).
N_b	Set of buses (b_1 *to* b_e).
N_{Br}	Set of branches.
N_{z_k}	Set of vulnerable branches at zone z_k.
z_1 *to* z_s	Set of geographical zones.

Parameters:

ξ_{z_k}	Cardinality budget of zone z_k.
$\Delta^S_{i,t}, \Delta^W_{i,t}, \Delta^D_{i,t}$	Deviation of $\tilde{P}^S_{i,t}, \tilde{P}^W_{i,t}$, and $\tilde{P}^D_{i,t}$ from $\bar{P}^S_{i,t}, \bar{P}^W_{i,t}$ and $\bar{P}^D_{i,t}$, respectively.
$\bar{P}^S_{i,t}, \bar{P}^W_{i,t}, \bar{P}^D_{i,t}$	Forecasted solar plant power, forecasted wind plant power, and forecasted load at bus i and time t.
Γ_t	Budget of uncertainty at time t.
$N_{P,ij}$	Number of poles in branch ij.
w_m	Maximum forecasted wind speed.
t_k	Time period in which windstorm reaches zone k.
$VOLL$	Value of loss load [$/MWh].
$O^G_i/O^W_i/O^S_i$	Generation cost of dispatchable/wind/solar generator at bus i [$/MWh].
O^{US}_t	Price of purchasing energy from the upstream grid [$/MWh].
O^D_t	Price of selling energy to consumers [$/MWh].
$PF^D_{i,t}$	Load power factor at bus i and time t.
g_{ij}, b_{ij}	Conductance and susceptance of branch ij [p.u].
$\alpha_{ij,t,n}, \beta_{ij,t,n}$	Coefficients used for the segment n of the piecewise linearization of $\cos(\theta_{i,t} - \theta_{j,t})$.
SC^{su}_i/SC^{sd}_i	Start-up/shut-down cost of dispatchable generator at bus i [$].
η^{ES}_i	Conversion efficiency of energy storage system at bus i, equal for charging and discharging.
E^{ES}_i	Capacity of energy storage system at bus i [MWh].
$SOC^{ES}_{i,limit}$	State of charge limit for energy storage system at bus i (%).
M	Big M value

Manuscript received April 8, 2019; revised September 17, 2019; accepted February 25, 2020. Date of publication March 2, 2020; date of current version August 24, 2020. Paper no.-TPWRS-00511-2019. *(Corresponding author: Nima Amjady.)*

Moein Esfahani, Nima Amjady, and Bahareh Bagheri are with the Department of Electrical Engineering, Semnan University, Semnan 98 23, Iran (e-mail: m.esfahani@semnan.ac.ir; amjady@semnan.ac.ir; b.bagheri@semnan.ac.ir).

Nikos D. Hatziargyriou is with the National Technical University of Athens, Athens 157 73, Greece (e-mail: nh@power.ece.ntua.gr).

Color versions of one or more of the figures in this article are available online at http://ieeexplore.ieee.org.

Digital Object Identifier 10.1109/TPWRS.2020.2977405

$\tilde{C}^{l}_{ij,t}$	Binary uncertain parameter that is 1 if branch ij at time t is under windstorm-caused contingency and 0 otherwise.
$\tilde{P}^{S}_{i,t}, \tilde{P}^{W}_{i,t}, \tilde{P}^{D}_{i,t}$	Uncertain solar plant power, uncertain wind plant power, and uncertain demand at bus i and time t.
$\hat{C}^{l}_{ij,t}$	The value of $\tilde{C}^{l}_{ij,t}$ obtained from the LS.
$\hat{P}^{S}_{i,t}, \hat{P}^{W}_{i,t}, \hat{P}^{D}_{i,t}$	The values of $\tilde{P}^{S}_{i,t}, \tilde{P}^{W}_{i,t}$, and $\tilde{P}^{D}_{i,t}$ obtained from the BCD second sub-problem.
ε^{BCD}	Convergence tolerance for BCD loop.

Variables:

ρ_{ij}	Outage probability of branch ij.
$\rho_{ij,l}$	Outage probability of branch ij due to conductor failure.
$\rho_{ij,p}$	Outage probability of branch ij due to pole failure.
ρ_{p-ind}	Individual pole failure probability.
$z^{S}_{i,t}, z^{W}_{i,t}, z^{D}_{i,t}$	Auxiliary continuous variables used to model the uncertain parameters $\tilde{P}^{S}_{i,t}$, $\tilde{P}^{W}_{i,t}$ and $\tilde{P}^{D}_{i,t}$.
$P^{sh}_{i,t}$	Active power shedding at bus i at time t [p.u.].
$v_{i,t}$	Voltage magnitude of bus i at time t [p.u.].
$P_{ij,t}/Q_{ij,t}/S_{ij,t}$	Active/Reactive/Apparent power flow of branch ij at time t [p.u.].
$P^{US}_{t}/Q^{US}_{t}/S^{US}_{t}$	Active/Reactive/Apparent power received from upstream grid at time t [p.u.].
$P^{W/S/G}_{i,t}$	Active power generation of wind/solar/dispatchable generators at bus i and time t [p.u.].
$C^{su}_{i,t}/C^{sd}_{i,t}$	Start-up/shut-down cost of dispatchable generator at bus i and time t ($).
$\theta_{i,t}$	Voltage angle of bus i at time t [rad].
$\omega_{ij,t}$	Piecewise linear approximation of $\cos(\theta_i - \theta_j)$.
$u^{\omega}_{ij,t,n}/\Delta\theta_{ij,t,n}$	Binary/continuous variable used for linear approximation of $\cos(\theta_{i,t} - \theta_{j,t})$.
$u^{G}_{i,t}$	Binary variable that is 1 if dispatchable unit at bus i and time t is committed and 0 otherwise.
$SOC^{ES}_{i,t}$	State of charge of energy storage system at bus i and time t (%).
$u^{ES}_{i,t}$	Binary variable that is 1/0 if energy storage system at bus i and time t is charging/discharging.
$FB^{\gamma,\lambda,\nu}$	BCD first sub-problem objective.
$\mu^{S}_{ij,t}, \mu^{W}_{ij,t}, \mu^{D}_{ij,t}$	Dual variables associated with the generation capacity of solar plant, generation capacity of wind plant, and load demand.

I. Introduction

A. Motivation

IN RECENT years, natural disasters, such as floods, windstorms, hurricanes and other weather-related incidents have increased gradually due to global climate changes. These natural events have imposed severe damages and financial losses in electrical power systems. For instance, between 1980 and 2014, 178 catastrophic natural events occurred around the world with total costs of over one trillion dollars [1]. Also, from 2003 to 2012, power system outages caused by natural disasters covered 58% of US grid outages and cost an annual average of 18 to 33 billion dollars [2]. These high-impact low-probability (HILP) natural events cannot be appropriately evaluated by traditional reliability measures.

Power system resilience is the ability of the system to mitigate the impacts of HILP natural events by deploying operational enhancement and infrastructural reinforcement measures. Despite the fact that infrastructural hardening measures have a great impact on power grid resilience, operational techniques provide a capability to proactively manage the system performance against the natural disasters [3]. Due to recent increasing rate of windstorm occurrence around the world and inherent density of power distribution grids, which makes them vulnerable against intensive disruptions, this paper focuses on operational resilience enhancement of active distribution networks against windstorms.

B. Literature Review

From time-scale point of view, resilience improvement comprises measures at the planning and measures at the operational stage. Planning-oriented measures aim to make the infrastructure less vulnerable to HILP events with different hardening strategies [3]. In [4] a hardening strategy for resilience enhancement has been proposed considering the uncertainty of out-of-service lines. The problem is presented as a bi-level optimization problem and is transformed into a single-level one using KKT conditions.

Operational-oriented measures, in addition to mitigating the consequences of HILP events, can provide an insight into the network vulnerability [3], [5]. Since HILP events are not frequent, historical data cannot be used to estimate their likelihood. Thus, it is more appropriate to consider their uncertain impacts on the network. Accordingly, it is essential to implement an appropriate model to simulate a particular HILP event and analyze its impacts on the system. This model should predict the system vulnerability against an event and should provide an insight for DSOs about upcoming consequences and help them to proactively manage them [6].

Different operational-oriented resilience-enhancement approaches for distribution systems have been recently presented in the literature. In [7] a two-stage stochastic programming method for optimal scheduling of micro-grids (MGs) has been proposed to mitigate load shedding of contingencies. A two-stage critical load restoration framework has been proposed in [8] to coordinate distributed local resources, such as distributed generators and microgrids. Its strategy tends to restore a maximum number of prioritized critical loads on distribution feeders to lessen the consequences of a major outage caused by a catastrophic event. Another resilient restoration approach has been presented in [9] that searches for different restoration paths with the aid of tie-switches and considers time-dependent distributed energy

resources (DERs), in order to optimize their restoration time and the number of critical loads to be picked up. In [10] a multi-objective model has been presented to maximize the resilience of an interdependent system and to minimize the total cost of restoration. The method considers the limitation of available recourses as well as the availability of maintenance crews and selects the best prioritized restoration strategy for different disruption scenarios. The uncertainties of infrastructure repair time and DERs' limitations have been considered in [11] and a scenario tree approximation has been employed to capture the stochastic behavior of these uncertain parameters. A two-stage stochastic problem has been formulated, which has been solved via tailored Benders Decomposition algorithm. Also, [12] has presented a service restoration method for MGs considering the continuous operation time (COT). Then, it has formulated the critical load restoration problem as a two stage heuristic using Markov-chain-based operation model. In [13] a mixed-integer linear programming approach using a distributed multi-agent coordination scheme is presented to maximize the support of critical loads. In [14] a two-stage robust optimization approach is presented to improve the resilience of integrated power distribution and natural gas networks. This problem is solved via column-and-constraint generation (C&CG) algorithm.

Resilience measures can be influenced by the type of natural disasters since a power system may be resilient against one natural disaster but could be vulnerable against other types [5]. In [15] a stochastic programming approach is proposed for enhancing the resilience of distribution systems against wildfires considering the dynamic line rating of overhead lines as well as the uncertainties of solar radiation, wind speed, and wind direction. In [16] smart operational resilience improvements against windstorms have been proposed based on resilience trapezoid concept and wind-dependent failure probability of transmission lines and poles. Furthermore, in [17] a proactive framework has been presented in order to operationally manage the impacts of extreme windstorms. That framework searches for a pre-event schedule with the minimum number of in-service vulnerable branches obtained from mapping the wind profile into fragility curve of each branch. In line with these research works, this paper focuses on the operational resilience enhancement of distribution networks to provide an insight into upcoming windstorm and increase the preparedness and robustness of the network against it. Using the proposed operation resiliency enhancement approach, distribution system operators can plan a more effective day-ahead operation strategy to cope with windstorms with a lower total cost.

During an incident, distribution system operators (DSOs) can commit micro-turbines (MTs) and energy storage systems (ESSs) to cope with the natural disaster consequences [15]. In [14] two-stage robust optimization models have been presented for resilience problems with commitment variables in the first stage of the decision-making process as *here-and-now* decisions. However, MTs and ESSs usually have a fast response time. For instance, General Electric LM6000 turboshaft gas turbine unit can start and reach its maximum power in 5 minutes [18]. Thus, these commitment variables can be considered in the second stage of the decision-making process as *wait-and-see* decisions to provide more flexibility as these decisions can be made based on the prevailing conditions.

C. Contributions and Paper Organization

The main contributions of this paper can be summarized as:

1) Introducing zonal wind-speed-specific uncertainty sets to model the uncertain parameters associated with windstorms. Unlike [14], [19] which consider zonal uncertainty sets for all branches, this paper explicitly determines the cardinality budget with respect to windstorm intensity at each zone and searches for the worst-case contingency among the identified vulnerable branches. In this way, the worst-case contingency associated with each windstorm can be more effectively determined.
2) A robust resilience-oriented operation scheduling model for active distribution networks is presented. The proposed model optimizes the binary commitment variables of MTs and ESSs as the second-stage (*wait-and-see*) decisions in the decision making process. In this way, the proposed ROUC model can employ the quick start capability of these units to provide more flexibility to cope with windstorm-caused contingencies.
3) A new solution approach based on block coordinate descent (BCD) and line search (LS) is proposed to solve the robust resilience-oriented operation scheduling problem. Unlike the conventional duality-based and KKT-based solution methods, the proposed approach can solve robust optimization problems with binary decision variables in the second level. In addition, the proposed BCD+LS solution method can extract the worst-case realization considering both binary and continuous uncertain parameters as well as their interactions.

The rest of this paper is organized as follows. In Section II, the proposed uncertainty modeling approach is introduced. Section III presents the robust resilience-oriented operation scheduling model for active distribution networks. The proposed solution method is detailed in Section IV. The results obtained from the proposed model and solution method are presented in Section V and compared with the results obtained from alternative methods. Section VI concludes the paper.

II. The Proposed Uncertainty Modeling Approach

The uncertainties considered in this paper include the windstorm-caused contingencies as well as the uncertainties of load demand, wind power, and solar power forecasts.

Wind speed is the most destructive force of a windstorm. Based on the geographical location of a windstorm, the consequent high winds mostly have a specific direction and path. According to national oceanic and atmospheric administration (NOAA) storm database [20], as windstorm drifts away from the high-pressure point, the wind speed gradually decreases along its path. Thus, in order to capture the spatiotemporal dynamics of windstorms, multi-zone and multi-stage uncertainty set needs to be determined [21]. Accordingly, the distribution system is divided into different zones based on the windstorm path and geographical location of power branches. Overhead lines and

distribution poles subject to the maximum predicted wind speed are the most vulnerable components of each zone. As a result of mapping maximum predicted wind speed to the fragility curves of lines and poles in each zone, the failure probability of each branch in each zone can be derived. The branch failure probability is formulated as follows [22], [23]:

$$\rho_{ij}\left(w_m\right) = \rho_{ij,l}\left(w_m\right) + \rho_{ij,p}\left(w_m\right) - \rho_{ij,l}\left(w_m\right)\rho_{ij,p}\left(w_m\right) \tag{1}$$

$$\rho_{ij,p}\left(w_m\right) = 1 - \left(1 - \rho_{p-ind}\left(w_m\right)\right)^{N_{P,ij}} \tag{2}$$

As illustrated in (1) a branch fails if one of its poles or its distribution line fails. If the maximum failure probability of each branch exceeds the vulnerability threshold, the branch is considered as vulnerable. The vulnerability threshold is the result of a compromise between the operation cost and the solution conservatism. The total number of vulnerable branches in each zone is considered as the cardinality budget of that zone. Notably, each geographical zone of a distribution network has a different forecasted wind speed and a different cardinality budget.

After determining the vulnerable branches of each zone, the multi-stage and multi-zone uncertainty set is determined using the vulnerable branches with a sophisticated but more realistic cardinality budget for each geographical zone. Thus, the wind-speed-specific uncertainty set U_w is formulated as follows:

$$\begin{aligned}
U_w = \Bigg\{ & \tilde{C}^l_{ij,t} \in \{0,1\} \mid \sum_{ij \in N_{z_1}} \tilde{C}^l_{ij,t_1} \le \xi_{z_1}, \\
& \tilde{C}^l_{ij,t_1} = 0,\ \forall (ij) \in \{N_{Br} \backslash N_{z_1}\}, \\
& \qquad \sum_{ij \in N_{z_2}} \tilde{C}^l_{ij,t_2} \le \xi_{z_2}, \\
& \tilde{C}^l_{ij,t_2} = \tilde{C}^l_{ij,t_1},\ \forall (ij) \in \{N_{Br} \backslash N_{z_2}\}, \\
& \qquad \cdots \\
& \qquad \sum_{ij \in N_{z_s}} \tilde{C}^l_{ij,t_s} \le \xi_{z_s}, \\
& \tilde{C}^l_{ij,t_s} = \tilde{C}^l_{ij,t_{s-1}},\ \forall (ij) \in \{N_{Br} \backslash N_{z_s}\} \Bigg\}
\end{aligned} \tag{3}$$

$\tilde{C}^l_{ij,t}$ is equal to 0 for all non-vulnerable branches in order to exclude them from the proposed uncertainty set. In addition, the relation between $\tilde{C}^l_{ij,t}$ values of the branches in each zone and the cardinality budget of that zone is given in (3). In general, for zone s, the part $\sum_{ij \in N_{z_s}} \tilde{C}^l_{ij,t_s} \le \xi_{z_s}$ specifies that the number of contingencies in Zone s is limited by the cardinality budget ξ_{z_s}. Also, $\{N_{Br} \backslash N_{z_s}\}$ is the set of branches that are not located in Zone s. Hence, the part $\tilde{C}^l_{ij,t_s} = \tilde{C}^l_{ij,t_{s-1}}, \quad \forall (ij) \in \{N_{Br} \backslash N_{z_s}\}$ means that the branches not located in Zone s will remain in the same state as they were in the previous period $t_s - 1$. For zone 1, the part $\tilde{C}^l_{ij,t_s} = \tilde{C}^l_{ij,t_{s-1}}, \quad \forall (ij) \in \{N_{Br} \backslash N_{z_s}\}$ becomes $\tilde{C}^l_{ij,t_1} = 0, \quad \forall (ij) \in \{N_{Br} \backslash N_{z_1}\}$, since in period t_1 the windstorm has not reached the next zones yet.

The uncertainty set U_w differs from previous multi-zone and multi-stage uncertainty sets (presented, e.g., in [14], [21]) by two important differences: 1) Based on the identified vulnerable branches of each zone, U_w models the impacts of a windstorm as "$N-K$" worst-case contingency, 2) Instead of randomly selecting the cardinality budgets, $\xi_{z_1}, \ldots, \xi_{z_s}$ in U_w are selected based on the windstorm-specific failure probabilities.

Other uncertainty sources pertaining to load demand, wind power and solar power are characterized by polyhedral uncertainty set as:

$$\bar{P}^S_{i,t} - z^S_{i,t}\Delta^S_{i,t} \le \tilde{P}^S_{i,t} \le \bar{P}^S_{i,t} + z^S_{i,t}\Delta^S_{i,t}, \ \ i \in N_b,\ t \in T \tag{4}$$

$$\bar{P}^W_{i,t} - z^W_{i,t}\Delta^W_{i,t} \le \tilde{P}^W_{i,t} \le \bar{P}^W_{i,t} + z^W_{i,t}\Delta^W_{i,t}, \quad i \in N_b,\ t \in T \tag{5}$$

$$\bar{P}^D_{i,t} - z^D_{i,t}\Delta^D_{i,t} \le \tilde{P}^D_{i,t} \le \bar{P}^D_{i,t} + z^D_{i,t}\Delta^D_{i,t}, \quad i \in N_b,\ t \in T \tag{6}$$

$$z^S_{i,t}, z^W_{i,t}, z^D_{i,t} \in [0,1], \quad i \in N_b,\ t \in T \tag{7}$$

$$\sum_{i \epsilon N_b} \left(z^S_{i,t} + z^W_{i,t} + z^D_{i,t}\right) \le \Gamma_t,\ t \in T \tag{8}$$

The degree of robustness of the proposed model against uncertain continuous parameters can be controlled using the bounded intervals given in (4)-(6) as well as the budget of uncertainty defined in (8).

III. Proposed Robust Resilience-Oriented Operation Scheduling Model

In this section, deterministic Resiliency-Oriented Unit Commitment (ROUC) model is first presented. Then, using this deterministic ROUC, the proposed robust ROUC model is introduced.

A. Deterministic ROUC

Deterministic ROUC model of an active distribution network can be formulated as:

$$\begin{aligned}
\min_{DV} \sum_{t \epsilon T} \Bigg(& \sum_{i \epsilon N_b} \left(VOLL \cdot P^{sh}_{i,t}\right) + \left(O^G_i \cdot P^G_{i,t}\right) + \left(O^W_i \cdot P^W_{i,t}\right) \\
& + \left(O^S_i \cdot P^S_{i,t}\right) + \left(C^{su}_{i,t} + C^{sd}_{i,t}\right) \\
& + \left(O^{US}_t \cdot P^{US}_t\right) - O^D_t \cdot \left(\bar{P}^D_{i,t} - P^{sh}_{i,t}\right) \Bigg)
\end{aligned} \tag{9}$$

s.t.

$$\sum_{j=b_1}^{b_e} P_{ij,t} = P^G_{i,t} + P^W_{i,t} + P^S_{i,t} - P^{Ch}_{i,t} + P^{Dh}_{i,t} + P^{US}_t - \bar{P}^D_{i,t} + P^{sh}_{i,t}, \ \ i \in N_b,\ ij \in N_{Br},\ t \in T \tag{10}$$

$$\sum_{j=b_1}^{b_e} Q_{ij,t} = Q^G_{i,t} + Q^{ES}_{i,t} + Q^{US}_t - \left(\bar{P}^D_{i,t} \cdot PF^D_{i,t}\right) + \left(P^{sh}_{i,t}\Delta PF^D_{i,t}\right), \quad i \in N_b,\ ij \in N_{Br},\ t \in T \tag{11}$$

$$0 \le P^W_{i,t} \le \bar{P}^W_{i,t}, \quad i \in N_b,\ t \in T \tag{12}$$

$$0 \le P^S_{i,t} \le \bar{P}^S_{i,t}, \quad i \in N_b,\ t \in T \tag{13}$$

$$0 \le P^{sh}_{i,t} \le \bar{P}^D_{i,t}, \quad i \in N_b,\ t \in T \tag{14}$$

$$0 \le S_{ij,t} \le S_{ij}^{\max}, \quad ij \in N_{Br},\ t \in T \tag{15}$$

$$P_{ij,t} = g_{ij} \cdot (v_{i,t} - v_{j,t} - \omega_{ij,t} + 1) - b_{ij} \cdot (\theta_{i,t} - \theta_{j,t}),$$
$$i,j \in N_b, ij \in N_{Br},\ t \in T \tag{16}$$

$$Q_{ij,t} = -b_{ij}\Delta\,(v_{i,t} - v_{j,t} - \omega_{ij,t} + 1) - g_{ij} \cdot$$
$$(\theta_{i,t} - \theta_{j,t}),\ i \in N_b, ij \in N_{Br},\ t \in T \tag{17}$$

$$\sum_n \Delta\theta_{ij,t,n} = \theta_{i,t} - \theta_{j,t},\ i \in N_b, ij \in N_{Br},\ t \in T \tag{18}$$

$$\omega_{ij,t} = \sum_n \left(\alpha_{ij,t,n}\Delta\theta_{ij,t,n} + u_{ij,t,n}^{\omega}\beta_{ij,t,n}\right),$$
$$ij \in N_{Br},\ t \in T \tag{19}$$

$$\sum_n u_{ij,t,n}^{\omega} = 1,\ ij \in N_{Br},\ t \in T \tag{20}$$

$$\Delta\theta_n^{\min} u_{ij,t,n}^{\omega} \le\ \Delta\theta_{ij,t,n} \le \Delta\theta_n^{\max} u_{ij,t,n}^{\omega},\ ij \in N_{Br},\ t \in T \tag{21}$$

$$P_i^{G,min}\ u_{i,t}^G \le\ P_{i,t}^G\ \le P_i^{G,max}\ u_{i,t}^G,\ i \in N_b,\ t \in T \tag{22}$$

$$Q_i^{G,min}\ u_{i,t}^G \le\ Q_{i,t}^G\ \le Q_i^{G,max}\ u_{i,t}^G,\ \ i \in N_b,\ t \in T \tag{23}$$

$$C_{i,t}^{su} \ge 0,\ C_{i,t}^{su} \ge SC_i^{su}\ \left(u_{i,t}^G - u_{i,t-1}^G\right),\ i \in N_b,\ t \in T \tag{24}$$

$$C_{i,t}^{sd} \ge 0,\ C_{i,t}^{sd} \ge SC_i^{sd}\ \left(u_{i,t-1}^G - u_{i,t}^G\right),\ i \in N_b,\ t \in T \tag{25}$$

$$0 \le S_t^{US} \le S^{US,max},\ \ t \in T \tag{26}$$

$$v_i^{\min} \le v_{i,t} \le v_i^{\max},\ \ i \in N_b,\ t \in T \tag{27}$$

$$SOC_{i,t}^{ES} = SOC_{i,t-1}^{ES} + \frac{\eta_i^{ES} P_{i,t}^{Ch}}{E_i^{ES}} - \frac{P_{i,t}^{Dh}}{\eta_i^{ES} E_i^{ES}},$$
$$i \in N_b,\ t \in T \tag{28}$$

$$SOC_i^{ES,min} \le SOC_{i,t}^{ES} \le SOC_i^{ES,max},\ \ i \in N_b,\ t \in T \tag{29}$$

$$SOC_{i,t_s}^{ES} \ge SOC_{i,limit}^{ES},\ i \in N_b \tag{30}$$

$$0 \le P_{i,t}^{Ch} \le P_i^{Ch,max} u_{i,t}^{ES},\quad i \in N_b,\ t \in T \tag{31}$$

$$0 \le P_{i,t}^{Dh} \le P_i^{Dh,max}\left(1 - u_{i,t}^{ES}\right),\quad i \in N_b,\ t \in T \tag{32}$$

$$Q_i^{ES,min} \le Q_{i,t}^{ES} \le Q_i^{ES,max},\quad i \in N_b,\ t \in T \tag{33}$$

Objective function (9) minimizes the total cost of an active distribution network minus the revenue of selling energy to the costumers. The total cost includes the load shedding cost, the generation cost of dispatchable, wind and solar generators, the startup and shut down costs of dispatchable units, and the purchased power cost. To maximize resilience of a distribution network, its lost load should be minimized [24]. Therefore, the first term in (9) represents the total load shedding cost. The decision variables of the deterministic ROUC, denoted by *DV* in (9), are as: $DV = \{u_{i,t}^G, P_{i,t}^G, Q_{i,t}^G, P_{i,t}^W, P_{i,t}^S, P_t^{US}, Q_t^{US}, u_{i,t}^{ES}, P_{i,t}^{Ch}, P_{i,t}^{Dh}, Q_{i,t}^{ES}\}$.

Equations (10) and (11) are active and reactive nodal balance constraints. For the boundary bus of the active distribution network, P_t^{US} and Q_t^{US} represent active and reactive powers received from the upstream grid. For the other buses, P_t^{US} and Q_t^{US} are zero. Constraints (12) and (13) are wind power and solar power limitations considering their spillages. Load shedding bounds are given in (14). Constraint (15) limits branch power flows. In this paper, the connection between apparent power flow and active and reactive power flows is linearized using polygonal linearization method [25]. Constraints (16)–(21) present piecewise linearized AC power flow equations [4]. Active and reactive output limits of dispatchable units are defined in (22) and (23). $P_i^{G,min}$ and $Q_i^{G,min}$ in (22) and (23) usually have nonzero values. Hence, without considering commitment variables, the OFF state of dispatchable units cannot be modeled and thus all dispatchable units should be in ON state in all hours of the scheduling horizon to satisfy (22) and (23). This can lead to non-optimal and even infeasible solutions for day-ahead operation planning [26]. Moreover, the proposed resiliency optimization framework is a day-ahead distribution operation planning model. Even if the units are disconnected in one hour by their dynamics and we should restart them, we still need commitment variables to plan operation of the units in the other hours of the next day. The constraints of the start-up and shut-down costs are given in (24) and (25). Power purchased from the upstream grid is limited in terms of the apparent power capacity of the boundary substation in (26). Voltage magnitude limits are in (27). State of charge (SOC) of energy storage systems (ESSs) is calculated in (28) and is limited in (29). Constraint (30) enforces the SOC of ESSs to be above a prespecified value at the end of the scheduling horizon. Charge and discharge constraints of ESSs, considering the operation mode, are given in (31) and (32). Reactive output limits of ESSs are specified in (33).

Although load shedding at distribution level is actually performed in a discrete manner, it has been modeled as a continuous variable in (9)–(33) due to the following reasons: 1) Disconnection of a single feeder typically leads to a very small load shedding compared to the total load of the distribution network, 2) Many distribution feeders are currently equipped with under-load interruptible disconnectors (or similar switches) and thus a part of the feeder's load can be interrupted. Therefore, the step of load shedding can be smaller than a feeder's load, 3) Even in load shedding or load transferring maneuvers routinely performed in distribution dispatch centers, the exact load shedding or load transferring amount may not be implementable. Thus, distribution dispatchers apply the closest load shedding or load transfer value. Accordingly, we assume that the same load shedding value determined by the proposed model or the closest practically implementable value to it would be applied by the associated distribution dispatch centers, and 4) a binary variable can be easily assigned to each distribution feeder in the proposed approach to exactly model the discrete nature of load shedding. However, this excessively increases the number of binary variables due to the large number of distribution feeders, which can make the proposed model intractable.

The deterministic ROUC model presented in (9)–(33) cannot characterize the forecast uncertainties of load and renewable generations as well as the equipment availability uncertainties pertaining to windstorm-caused contingencies. To solve this problem, the proposed robust ROUC model is introduced.

B. Proposed Bi-Level Robust ROUC Model

The proposed bi-level model intends to proactively manage and increase the resilience of an active distribution network against windstorms and immunize the network against the worst-case realization of windstorm-caused branch contingencies, load demands, wind powers and solar powers. The proposed bi-level model, which is the robust counterpart of ROUC model (9)–(33), is presented in (34)–(46):

$$\min_{DV} \max_{z^S_{i,t}, z^W_{i,t}, z^D_{i,t}, \tilde{C}^l_{ij,t}} \sum_{t \epsilon T} \Bigg(\sum_{i \epsilon N_b} \left(VOLL \cdot P^{sh}_{i,t}\right) + \left(O^G_i \cdot P^G_{i,t}\right) + \left(O^W_i \cdot P^W_{i,t}\right) + \left(O^S_i \cdot P^S_{i,t}\right) + \left(C^{su}_{i,t} + C^{sd}_{i,t} + \left(O^{US}_t \cdot P^{US}_t\right) - O^D_t \cdot \left(\tilde{P}^D_{i,t} - P^{sh}_{i,t}\right)\right) \Bigg) \quad (34)$$

s.t.

$$\sum_{j=b_1}^{b_e} P_{ij,t} = P^G_{i,t} + P^W_{i,t} + P^S_{i,t} - P^{Ch}_{i,t} + P^{Dh}_{i,t} + P^{US}_t - \tilde{P}^D_{i,t} + P^{sh}_{i,t}, \quad i \in N_b,\ ij \in N_{Br},\ t \in T \quad (35)$$

$$\sum_{j=b_1}^{b_e} Q_{ij,t} = Q^G_{i,t} + Q^{ES}_{i,t} + Q^{US}_t - \left(\tilde{P}^D_{i,t} \cdot PF^D_{i,t}\right) + \left(P^{sh}_{i,t} \cdot PF^D_{i,t}\right), \quad i \in N_b,\ ij \in N_{Br},\ t \in T \quad (36)$$

$$0 \le P^W_{i,t} \le \tilde{P}^W_{i,t}, \quad i \in N_b,\ t \in T \quad (37)$$

$$0 \le P^S_{i,t} \le \tilde{P}^S_{i,t}, \quad i \in N_b,\ t \in T \quad (38)$$

$$0 \le P^{sh}_{i,t} \le \tilde{P}^D_{i,t}, \quad i \in N_b,\ t \in T \quad (39)$$

$$0 \le S_{ij,t} \le S^{\max}_{ij} \left(1 - \tilde{C}^l_{ij,t}\right), \quad ij \in N_{Br},\ t \in T \quad (40)$$

$$-M \left(1 - \tilde{C}^l_{ij,t}\right) \le P_{ij,t} \le M \left(1 - \tilde{C}^l_{ij,t}\right) \quad (41)$$

$$-M \left(1 - \tilde{C}^l_{ij,t}\right) \le Q_{ij,t} \le M \left(1 - \tilde{C}^l_{ij,t}\right) \quad (42)$$

$$-M\, \tilde{C}^l_{ij,t} \le P_{ij,t} - \left(g_{ij} \left(v_{i,t} - v_{j,t} - \omega_{ij,t} + 1\right) - b_{ij} \left(\theta_{i,t} - \theta_{j,t}\right)\right) \le M \tilde{C}^l_{ij,t}, \quad i \in N_b,\ ij \in N_{Br},\ t \in T \quad (43)$$

$$-M\, \tilde{C}^l_{ij,t} \le Q_{ij,t} - \left(-b_{ij} \left(v_{i,t} - v_{j,t} - \omega_{ij,t} + 1\right) - g_{ij} \left(\theta_{i,t} - \theta_{j,t}\right)\right) \le M \tilde{C}^l_{ij,t}, \quad i \in N_b,\ ij \in N_{Br},\ t \in T \quad (44)$$

$$(18) - (33) \quad (45)$$

$$(3) - (8) \quad (46)$$

1) The first level of the proposed model minimizes the total cost while maximizing the resilience of the active distribution network with respect to the operational constraints and the worst-case realization of the uncertain parameters obtained from the second level problem. In (41)–(44), the impacts of contingency binary variables $\tilde{C}^l_{ij,t}$ are applied using the big-M linearization method. Equations (41)–(44) are converted into equalities (16) and (17) when the branch ij is not affected by the windstorm-caused contingency (i.e., $\tilde{C}^l_{ij,t} = 0$). Also, the M values are selected as the maximum permissible branch flows. It is worth mentioning that, unlike recently used tri-level adaptive-robust optimization models that consider commitment variables as *here-and-now* decisions, the proposed bi-level model makes commitment decisions dynamically as the windstorm impacts the network along its path. This capability allows DSOs to proactively manage the consequences of the windstorm and to enhance the survivability of the distribution network.
2) By maximizing the objective function over the uncertain parameters, the second level of the proposed model extracts the worst-case realization of the uncertainties regarding constraints (46) in order to maximize the robustness of the solution.

It is noted that the proposed ROUC model employs available forecast values of continuous uncertain parameters and the fragility curves of branches, thus it only uses practically available input data without assuming any perfect knowledge of the worst-case scenario in the future. The statistical dependence between the input random variables (including load demand, wind speed, and solar power) is modeled in the forecast process that feeds the proposed ROUC model. To do this, multi-variable ARMA (auto-regressive moving average) or ARMAX time series is employed in the forecast process to model the statistical dependency between the input random variables, as well as the intertemporal statistical dependencies [27].

IV. Solution Approach

In order to effectively solve the proposed bi-level robust ROUC model, a hybrid solution approach composed of BCD method and LS technique is presented. To apply BCD for solving the robust ROUC problem, the BCD first sub-problem [28] contains the total cost function subject to the operational constraints. However, for constructing the BCD second sub-problem [28], there is no analytical expression for the total cost objective in terms of the second-level variables. Thus, the first-order Taylor series expansion of total cost objective function with respect to differentiable continuous uncertain parameters is used to build the BCD second sub-problem. This approach extracts the worst-case realization of continuous uncertain parameters including load demands, wind powers and solar powers. However, since the binary uncertain statuses of windstorm-caused contingencies are not differentiable variables, LS technique [27] is employed to find the worst windstorm-caused contingencies considering the cardinality budget of each zone. BCD and LS methods are iteratively applied to extract the worst-case realization of

both continuous and binary uncertainty sources considering their interactions. The proposed hybrid solution approach is as:

LS problem:

$$\max_{\tilde{C}^{l,\gamma,\lambda}_{ij,t}} \sum_{t\epsilon T} \sum_{ij\in N_{z_k}} \left(\tilde{C}^{l,\gamma,\lambda}_{ij,t}\left(\psi^{\gamma,\lambda}_{ij,t} - \psi^{\gamma,\,0}_{ij,t}\right)\right) \tag{47}$$

$$(3)\ \begin{vmatrix} \tilde{C}^{l}_{ij,t_1} = \tilde{C}^{l,\gamma,\lambda}_{ij,t_1}, \ldots, \tilde{C}^{l}_{ij,t_s} = \tilde{C}^{l,\gamma,\lambda}_{ij,t_s} \\ N_{z_1} = N^{\gamma}_{z_1}, \ldots,\ N_{z_s} = N^{\gamma}_{z_s} \end{vmatrix} \tag{48}$$

BCD first sub-problem:

$$\begin{aligned} FB^{\gamma,\lambda,\nu} = \min_{DV} \sum_{t\epsilon T} \Bigg(& \sum_{i\epsilon N_b} \left(VOLL \cdot P^{sh,\gamma,\lambda,\nu}_{i,t}\right) \\ & + \left(O^{G}_{i} \cdot P^{G,\gamma,\lambda,\nu}_{i,t}\right) + \left(O^{W}_{i} \cdot P^{W,\gamma,\lambda,\nu}_{i,t}\right) + \left(O^{S}_{i} \cdot P^{S,\gamma,\lambda,\nu}_{i,t}\right) + \left(C^{su,\gamma,\lambda,\nu}_{i,t} + C^{sd,\gamma,\lambda,\nu}_{i,t}\right) + \left(O^{US}_{t} \cdot P^{US,\gamma,\lambda,\nu}_{t} - O^{D}_{t} \cdot \left(\tilde{P}^{D,\gamma,\lambda,\nu}_{i,t} - P^{sh,\gamma,\lambda,\nu}_{i,t}\right)\right)\Bigg) \end{aligned} \tag{49}$$

s.t.

$$(35)\text{–}(45)\ \begin{vmatrix} P_{ij,t} = P^{\gamma,\lambda,\nu}_{ij,t},\ P^{G}_{i,t} = P^{G,\gamma,\lambda,\nu}_{i,t}, \\ P^{W}_{i,t} = P^{W,\gamma,\lambda,\nu}_{i,t},\ P^{S}_{i,t} = P^{S,\gamma,\lambda,\nu}_{i,t} \\ P^{Ch}_{i,t} = P^{Ch,\gamma,\lambda,\nu}_{i,t},\ P^{Dh}_{i,t} = P^{Dh,\gamma,\lambda,\nu}_{i,t}, \\ P^{US}_{t} = P^{US,\gamma,\lambda,\nu}_{t} \\ P^{sh}_{i,t} = P^{sh,\gamma,\lambda,\nu}_{i,t}, \tilde{P}^{D}_{i,t} = \tilde{P}^{D,\gamma,\lambda,\nu}_{i,t}, \\ \tilde{P}^{S}_{i,t} = \tilde{P}^{S,\gamma,\lambda,\nu}_{i,t}, Q^{G}_{i,t} = Q^{G,\gamma,\lambda,\nu}_{i,t}, \\ \tilde{P}^{W}_{i,t} = \tilde{P}^{W,\gamma,\lambda,\nu}_{i,t},\ \tilde{C}^{l}_{ij,t} = \tilde{C}^{l,\gamma,\lambda}_{ij,t}, \\ Q^{ES}_{i,t} = Q^{ES,\gamma,\lambda,\nu}_{i,t}, \\ Q^{US}_{t} = Q^{US,\gamma,\lambda,\nu}_{t},\ Q_{ij,t} = Q^{\gamma,\lambda,\nu}_{ij,t}, \\ S_{ij,t} = S^{\gamma,\lambda,\nu}_{ij,t}, \theta_{i,t} = \theta^{\gamma,\lambda,\nu}_{i,t}, \\ S^{US}_{t} = S^{US,\gamma,\lambda,\nu}_{t},\ \omega_{ij,t} = \omega^{\gamma,\lambda,\nu}_{ij,t}, \\ \Delta\theta_{ij,t,n} = \Delta\theta^{\gamma,\lambda,\nu}_{ij,t,n} \\ v_{i,t} = v^{\gamma,\lambda,\nu}_{i,t}, u^{\omega}_{ij,t,n} = u^{\omega,\gamma,\lambda,\nu}_{ij,t,n}, \\ C^{sd}_{i,t} = C^{sd,\gamma,\lambda,\nu}_{i,t}, C^{su}_{i,t} = C^{su,\gamma,\lambda,\nu}_{i,t} \\ u^{G}_{i,t} = u^{G,\gamma,\lambda,\nu}_{i,t}, SOC^{ES}_{i,t} = SOC^{ES,\gamma,\lambda,\nu}_{i,t}, \\ u^{ES}_{i,t} = u^{ES,\gamma,\lambda,\nu}_{i,t} \end{vmatrix} \tag{50}$$

$$\tilde{P}^{D,\gamma,\lambda,v}_{i,t} = \hat{P}^{D,\gamma,\lambda,v-1}_{i,t} : \mu^{D,\gamma,\lambda,v}_{i,t},\ i \in N_b,\ t \in T \tag{51}$$

$$\tilde{P}^{S,\gamma,\lambda,v}_{i,t} = \hat{P}^{S,\gamma,\lambda,v-1}_{i,t} : \mu^{S,\gamma,\lambda,v}_{i,t},\ i \in N_b,\ t \in T \tag{52}$$

$$\tilde{P}^{W,\gamma,\lambda,v}_{i,t} = \hat{P}^{W,\gamma,\lambda,v-1}_{i,t} : \mu^{W,\gamma,\lambda,v}_{i,t},\ i \in N_b,\ t \in T \tag{53}$$

$$\tilde{C}^{l,\gamma,\lambda}_{ij,t} = \hat{C}^{l,\gamma,\lambda}_{ij,t},\ ij \in N_{Br},\ t \in T \tag{54}$$

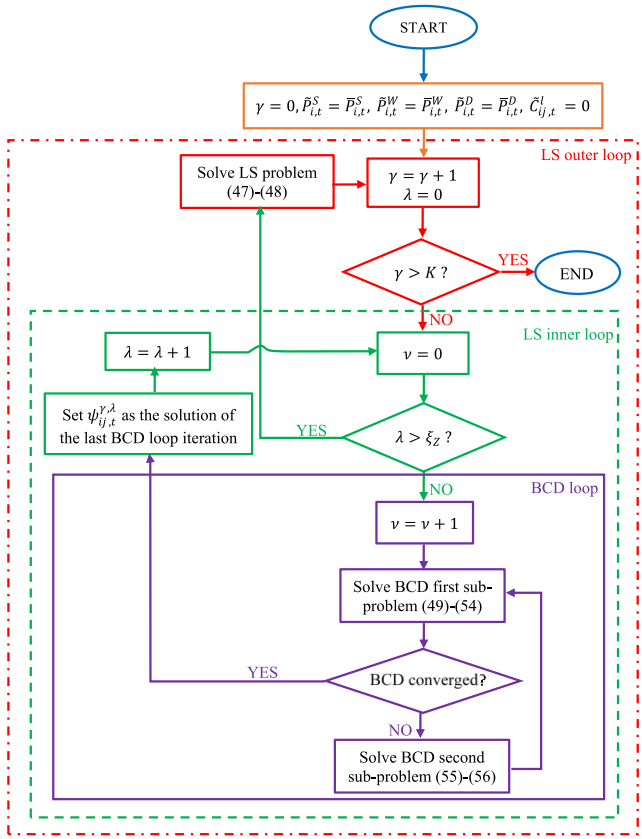

Fig. 1. Flowchart of the proposed solution method.

BCD second sub-problem:

$$\begin{aligned} \max_{\tilde{P}^{S}_{i,t},\, \tilde{P}^{W}_{i,t}, \tilde{P}^{D}_{i,t}} \Bigg[& FB^{\gamma,\lambda,\nu} + \\ & \sum_{t\epsilon T} \sum_{i\in\epsilon N_i} \left(\mu^{S,\gamma,\lambda,v}_{i,t}\left(\tilde{P}^{S,\gamma,\lambda}_{i,t} - \hat{P}^{S,\gamma,\lambda,v-1}_{i,t}\right)\right) \\ & + \mu^{W,\gamma,\lambda,v}_{i,t}\left(\tilde{P}^{W,\gamma,\lambda}_{i,t} - \hat{P}^{W,\gamma,\lambda,v-1}_{i,t}\right) \\ & + \mu^{D,\gamma,\lambda,v}_{i,t}\left(\tilde{P}^{D,\gamma,\lambda}_{i,t} - \hat{P}^{D,\gamma,\lambda,v-1}_{i,t}\right)\Bigg)\Bigg] \end{aligned} \tag{55}$$

s.t.

$$(4)\text{–}(8)\ \begin{vmatrix} \tilde{P}^{S}_{i,t} = \tilde{P}^{S,\gamma,\lambda,\nu}_{i,t},\ \tilde{P}^{W}_{i,t} = \tilde{P}^{W,\gamma,\lambda,\nu}_{i,t}, \\ \tilde{P}^{D}_{i,t} = \tilde{P}^{D,\gamma,\lambda,\nu}_{i,t} \\ z^{S}_{i,t} = z^{S,\gamma,\lambda,\nu}_{i,t},\ z^{W}_{i,t} = z^{W,\gamma,\lambda,\nu}_{i,t},\ z^{D}_{i,t} = z^{D,\gamma,\lambda,\nu}_{i,t} \end{vmatrix} \tag{56}$$

The proposed solution method, depicted above, comprises three nested loops as illustrated in the flowchart of Fig. 1. At first, the counter of the outermost loop and the uncertain parameters are initialized. The outermost loop in the proposed solution method is the LS outer loop which iteratively selects the K worst contingencies by considering the impacts of the previously selected worst contingencies. In this way, the "worst $N-K$ contingency" is selected by taking into account the interactions among contingencies, which leads to selecting a more critical "worst $N-K$ contingency" and thus providing

more immunization against the windstorm. This capability of the proposed solution method is numerically shown in the next section.

Selecting the worst branch contingency in each iteration of the LS outer loop is based on the LS inner loop in which a sensitivity analysis is performed to determine the impact of each branch failure on the objective function as shown in (47). The $\psi_{ij,t}^{\gamma,\,0}$ value is obtained when all vulnerable branches of $N_{z_1}^{\gamma},\ldots,N_{z_s}^{\gamma}$ are in service and $\psi_{ij,t}^{\gamma,\lambda}$ value is obtained when the vulnerable branch in the iteration γ/λ of the LS outer/inner loop is removed. After performing this sensitivity analysis (i.e., determining $\psi_{ij,t}^{\gamma,\lambda}-\psi_{ij,t}^{\gamma,\,0}$) for all branch failures in the LS inner loop, the objective given in (47) is maximized subject to (48) in the LS outer loop. The constraints (48) are the constraints (3) in which $\tilde{C}_{ij,t_1}^{l},\ldots,\tilde{C}_{ij,t_s}^{l}$ are replaced by their values in the iteration γ/λ of the LS outer/inner loop (i.e., $\tilde{C}_{ij,t_1}^{l,\gamma,\lambda},\ldots,\tilde{C}_{ij,t_s}^{l,\gamma,\lambda}$) and $N_{z_1},\ldots,N_{z_s}$ are replaced by their values in the iteration γ of the LS outer loop (i.e., $N_{z_1}^{\gamma},\ldots,\ N_{z_s}^{\gamma}$).

The LS inner loop is iterated by the cardinality budget of each zone to determine the worst branch contingency considering the previously selected worst contingencies. In other words, $N_{z_1}^{\gamma},\ldots,\ N_{z_s}^{\gamma}$ are updated in each iteration γ by removing the branches of the previously selected worst contingencies. The LS outer loop is iterated by K to determine "worst $N-K$ contingency".

In each iteration of the LS inner loop, the BCD loop is run. Each BCD loop iteration consists of solving the BCD first and second sub-problems. The BCD first sub-problem (49)–(54) determines the optimal solution in terms of the decision variables, considering fixed values for the continuous uncertain parameters. These fixed values are obtained from the BCD second sub-problem results in the previous BCD iteration $v-1$ as shown in (51)–(53). The binary uncertain parameters in the BCD first sub-problem are set based on the LS results as shown in (54). The BCD second sub-problem finds the worst-case realization of the continuous uncertain parameters as shown in (55)–(56). To do this, the BCD second sub-problem constructs the first- order Taylor series expansion of the objective function, as given in (55), using the dual variables obtained in the BCD first sub-problem. In (50) and (56), the variables and parameters are substituted by their values in the iterations similar to what is explained for (48). The extended forms of (48), (50), and (56) are given in [29].

As shown in (56), the polyhedral uncertainty set of the continuous uncertain parameters is updated in each iteration of the LS method. In other words, the worst-case realization of demand and renewable generations is found by considering the topology changes enforced by the windstorm-caused contingencies. In this way, the interactions between the continuous and binary uncertain parameters are taken into account.

The BCD convergence criterion indicated in the flowchart of Fig. 1 is:

$$\left|FB^{\gamma,\lambda,\nu}-FB^{\gamma,\lambda,\nu-1}\right|/\left|FB^{\gamma,\lambda,\nu}\right|\leq\varepsilon^{BCD} \qquad (57)$$

where ε^{BCD} is a prespecified tolerance. After the BCD convergence, its result is returned as $\psi_{ij,t}^{\gamma,\lambda}$ to the LS inner loop as shown in Fig. 1. Using $\psi_{ij,t}^{\gamma,\lambda}$ values, which are passed from the BCD to the LS, as well as $\hat{C}_{ij,t}^{l,\gamma,\lambda}$ values in (54), which are passed from the LS to the BCD, the LS and BCD loops are connected.

Algorithm of the Proposed Solution Method.

1. Initialization: $\tilde{P}_{i,t}^{S}=\bar{P}_{i,t}^{S}$, $\tilde{P}_{i,t}^{W}=\bar{P}_{i,t}^{W}$, $\tilde{P}_{i,t}^{D}=\bar{P}_{i,t}^{D}$, $\tilde{C}_{ij,t}^{l}=0$, $\gamma=0$ and $\varepsilon^{BCD}=10^{-6}$.
2. Update LS outer loop index $\gamma=\gamma+1$ and set the LS inner loop iteration to $\lambda=0$.
3. **If** $\gamma>K$, **Stop**.
   Else, **Go to** step 4.
4. Set the BCD loop iteration $\nu=0$ and $FB^{\gamma,\lambda,\nu}=\infty$.
5. **If** $\lambda>\xi_Z$, **Go to** step 13.
   Else, **Go to** step 6.
6. Update the BCD loop iteration $\nu=\nu+1$.
7. Solve the BCD first sub-problem (49)–(54) and update $FB^{\gamma,\lambda,\nu}$, $\mu_{i,t}^{D,\gamma,\lambda,\,v}$, $\mu_{i,t}^{S,\gamma,\lambda,\,v}$, $\mu_{i,t}^{W,\gamma,\lambda,\,v}$.
8. Calculate BCD convergence $|FB^{\gamma,\lambda,\nu}-FB^{\gamma,\lambda,\nu-1}|/|FB^{\gamma,\lambda,\nu}|$.
9. **If** BCD convergence is lower than ε^{BCD} **Go to** step 11
   Else, Go to step 10.
10. Solve the BCD second sub-problem (55), (56) and update $\hat{P}_{i,t}^{S,\gamma,\lambda,\,v}$, $\hat{P}_{i,t}^{W,\gamma,\lambda,\,v}$, and $\hat{P}_{i,t}^{D,\gamma,\lambda,\,v}$ as well as $\tilde{P}_{i,t}^{S,\gamma,\lambda,\,v}$, $\tilde{P}_{i,t}^{W,\gamma,\lambda,\,v}$, and $\tilde{P}_{i,t}^{D,\gamma,\lambda,\,v}$.
11. Set $\psi_{ij,t}^{\gamma,\lambda}$ as the last BCD solution $FB^{\gamma,\lambda,\nu}$.
12. Update the LS inner loop $\lambda=\lambda+1$ and **Go to** step 4.
13. Solve the LS problem (47), (48) and update $\tilde{C}_{ij,t}^{l,\gamma,\lambda}$ and $\hat{C}_{ij,t}^{l,\gamma,\lambda}$then **Go to** step 2.

The proposed hybrid BCD+LS solution approach finds an optimal solution considering the worst $N-K$ windstorm-caused contingency as well as the worst-case realization of the continuous uncertain parameters (i.e., load demands and renewable generations) to maximize the operational resilience of an active distribution network. The pseudocode of the proposed solution algorithm is presented in the following.

The entire problem is finally formulated as a unified MILP problem without any decomposition, which can easily be solved by available MILP solvers.

V. Simulation Results

In this section, the results obtained from the proposed ROUC model and the proposed BCD+LS solution method for a modified IEEE 33-bus active distribution network are presented. The obtained solution presents the resilience-oriented optimal scheduling of the active distribution network for the next 24 hours encountering a windstorm. The required data for this test system is taken from [7], [15], [30]. In addition, the forecasted power of the wind turbines and the solar plant for the scheduling horizon are taken from [7], [15].

The radial IEEE 33-bus system is divided into three geographical zones based on the windstorm path and intensity as illustrated in Fig. 2. It is assumed that the windstorm impacts the network at the first hour of the scheduling horizon. In this

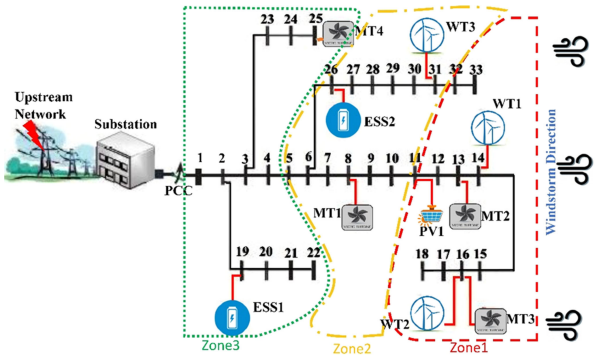

Fig. 2. Geographical zones of the IEEE 33-bus system.

TABLE I
THE RESULTS OBTAINED FROM THE PROPOSED ROUC MODEL, ARO, AND MODIFIED ARO

Case	Extracted Worst Contingencies	
	Proposed ROUC	ARO
Case I	12-13/14-15/16-17/32-33/7-8/10-11/6-26/30-31/2-3/24-25	11-12/14-15/16-17/32-33/5-6/10-11/6-26/30-31/2-3/21-22
Case II	12-13/14-15/16-17/10-11/6-26/30-31/2-3	11-12/14-15/16-17/5-6/10-11/30-31/2-3
Case III	12-13/14-15/15-16/16-17/32-33/7-8/10-11/6-26/30-31/2-3	11-12/13-14/14-15/16-17/32-33/5-6/10-11/6-26/30-31/2-3
Case IV	12-13/14-15/16-17/32-33/10-11/6-26/30-31/2-3	11-12/14-15/16-17/32-33/5-6/10-11/30-31/2-3

paper, according to the historical data of NOAA storm database [20], the maximum sustained wind speed is considered as 60 m/s for zone one, 55 m/s for zone two, and 50 m/s for zone three. The wind-dependent fragility curve of overhead distribution branches is taken from [22], [23]. Moreover, the cut-out speed of 25 m/s is considered for WTs in each zone. In addition, the vulnerability threshold is considered 0% [17] for the probabilistic vulnerability calculations presented in Section II. Using these calculations, overhead branches 11-12, 12-13, 14-15, 15-16, 16-17 and 32-33 in zone one, 5-6, 7-8, 10-11, 6-26, 30-31 and 31-32 in zone two and 2-3, 21-22 and 24-25 in zone three are identified as vulnerable branches. Therefore, the cardinality budget of zone one, two and three is 6, 6, and 3, respectively. The simulations of this paper are implemented in GAMS software package using CPLEX solver [31] on a Core i7 3.0 GHz laptop computer with 8 GB RAM. The relative optimality gap is considered 10^{-6} for CPLEX solver.

A. Evaluating the Results of the Proposed Bi-Level Robust ROUC Model

The results obtained from the proposed bi-level robust ROUC model, solved by the proposed BCD+LS solution method, are presented in Table I and are compared with the results of other alternatives. The total cost and computation time are reported for four different worst-contingency cases and five contingency cases are described in Table II. For instance, in the worst-contingency case I, a maximum of 4 branches in zone one, 4 branches in zone two, and 2 branches in zone three can be disconnected due to the contingency. The worst-contingency

TABLE II
DIFFERENT WORST-CONTINGENCY CASES

Case	Number of contingencies in (Zone 1, Zone 2, Zone 3)
I	(4,4,2)
II	(3,3,1)
III	(5,4,1)
IV	(4,3,1)

cases specified in Table II should be found within the cardinality budgets of the three zones, i.e., (6,6,3).

Since the test system has 32 loads, 3 wind turbines, and one solar plant, there are 36 continuous uncertain parameters in the robust ROUC model and thus Γ_t can vary in the range [0,36]. Five different Γ_t values in this range by the step of 25% (i.e., $0.25 \times 36 = 9$) are considered for the numerical experiments of Table I. As can be seen in Table I, as the robustness budget increases, the optimal total cost obtained from the proposed solution method increases. Also, increasing the number of contingencies from Case II to Case I directly impacts the total cost by increasing the loss of load.

To evaluate the linearization error caused by the linearization methods of the ROUC model, we have substituted the solution obtained by the linearized model in the original nonlinear equations. All original nonlinear equations have been satisfied with the linearized model solution with a negligible error around 0.2%. In addition, the linearization methods have been used to minimize the objective function in the outer "Min" problem of (34). However, the uncertainty ranges of the continuous uncertain parameters are used in the inner "Max" problem of (34) to find the worst-case realization. Accordingly, there is no need to consider any hypothesis on the uncertainty ranges regarding the linearization error.

B. Comparison With Tri-Level Adaptive Robust Optimization (ARO)

In this section, the results obtained from the proposed bi-level model and the recently presented tri-level ARO model [14], [19] are compared.

In contrast to the proposed bi-level model, the tri-level ARO model, in the form of *min-max-min*, consists of the following levels. The first level is to determine an optimal schedule for ESSs and MT units, subject to the extracted worst-case realization of uncertainties in the second level. Also, the third level is to minimize the total cost given the first level decisions and the worst-case realization of uncertainties obtained from the first and the second levels, respectively. The solution method for the tri-level ARO, is based on decomposing the tri-level model into a master problem and a sub-problem using primal cuts. Also, to solve the sub-problem, the duality-based transformation and big-M linearization are employed. Details of the ARO model and the decomposition-based solution method can be found in [32], [33].

As can be seen in Table I, the computation times of the proposed model are [2.35–2.78] times lower in case I and

TABLE III
EXTRACTED WORST CONTINGENCIES BY THE PROPOSED ROUC AND ARO ($\Gamma_t = 9$)

Case	Extracted Worst Contingencies	
	Proposed ROUC	ARO
Case I	12-13/14-15/16-17/32-33/7-8/10-11/6-26/30-31/2-3/24-25	11-12/14-15/16-17/32-33/5-6/10-11/6-26/30-31/2-3/21-22
Case II	12-13/14-15/16-17/10-11/6-26/30-31/2-3	11-12/14-15/16-17/5-6/10-11/30-31/2-3
Case III	12-13/14-15/15-16/16-17/32-33/7-8/10-11/6-26/30-31/2-3	11-12/13-14/14-15/16-17/32-33/5-6/10-11/6-26/30-31/2-3
Case IV	12-13/14-15/16-17/32-33/10-11/6-26/30-31/2-3	11-12/14-15/16-17/32-33/5-6/10-11/30-31/2-3

TABLE IV
SAMPLE MT SCHEDULING RESULTS OBTAINED FROM THE PROPOSED ROUC AND ARO FOR CASE I WITH $\Gamma_t = 9$

		Micro Turbines Status	
		On Times ($u^G_{i,t} = 1$)	Off times ($u^G_{i,t} = 0$)
Proposed ROUC	MT1	(t_2-t_{24})	(t_1-t_2)
	MT4	(t_3-t_{24})	(t_1-t_3)
ARO	MT1	(t_2-t_{24})	(t_1-t_2)
	MT4	(t_3-t_{24})	(t_1-t_2)
	MT2	(t_2-t_{24})	(t_1-t_2)

[2.65–2.77] times lower in case II compared to the computation times of the ARO model. The reason of this higher computational efficiency is that the proposed model determines the commitment variables and dispatch variables simultaneously considering their interactions. On the contrary, the tri-level ARO model solves the master problem to determine the optimal schedule of MTs and ESSs and then solves the sub-problem to determine the uncertainties and the dispatch variables.

Thus, the solution procedure of the tri-level ARO includes solving two massive problems in each iteration which increases the computation burden. In addition, it is worth mentioning that finding proper values for the big-M linearization parameters after the duality transformation of the sub-problem is a challenging task. In this paper, the big-M values are selected as tight as possible, since these values significantly impact the computation time and the solution quality of the ARO. In other words, the lowest computation times of the ARO, that we could obtain, have been reported in Table I.

From Table I, it seems that in contrast to the ARO, the proposed model has found a higher total cost. However, these different total costs are due to different worst contingencies (and thus different load shedding amounts) found by the ARO and the proposed model. To further evaluate this issue, the worst contingencies found by the proposed ROUC and ARO are shown in Table III. It is seen that different worst contingencies are extracted by the proposed ROUC and ARO as these two models use different contingency search procedures. Differences between the extracted worst contingencies in each case are specified by red color in Table III. To give a better insight about the severity of these two worst contingencies, sample MT scheduling results for case I with $\Gamma_t = 9$, obtained from the proposed ROUC and the ARO, are shown in Table IV. Note that, during a contingency, MTs can highly compensate the undesirable load shedding and thus evaluating the MT schedules obtained from each model is helpful to specify the severity of each worst contingency. Table IV shows that in the proposed ROUC, just MT_1 and MT_4 are committed during the windstorm. However, in the proposed ROUC, MT_2 and MT_3 are not committed since the contingency of branches 12-13, 14-15, 16-17 makes the load demand of MT_2 and MT_3 lower than their minimum output limits. On the contrary, since the ARO has extracted different worst contingencies 11-12, 14-15, 16-17, in which the minimum output limit for MT_2 is satisfied, this unit can be committed along with MT_1 and MT_4 in the ARO solution as indicated by red rectangle in Table IV. Therefore, compared to the ARO, the proposed ROUC has extracted more critical worst contingencies with a higher load shedding value. Consequently, the proposed ROUC has a higher total cost than the ARO since it immunizes the network against more critical worst contingencies. In other words, the ARO solution method does not consider the impacts of MT generations on the worst contingencies' selection and neglects the interaction between binary and continuous uncertain parameters. Hence, the ARO algorithm finds less critical contingencies compared with the proposed ROUC.

TABLE V
THE OUT-OF-SAMPLE ANALYSIS RESULTS FOR THE PROPOSED ROUC AND ARO

Solution Method	Fixed Worst Contingencies	Total Cost ($)			
		Case I	Case II	Case III	Case IV
Proposed	ARO	65468.139	63472.453	64997.245	64002.287
ARO	Proposed	67601.076	65199.148	67021.920	66924.349

To further evaluate the performance of the proposed ROUC and the ARO, a kind of out-of-sample analysis is presented here in which the ARO finds the optimal total cost given the worst contingencies extracted by the proposed ROUC and vice versa. Table V shows the results of this out-of-sample analysis for all cases with $\Gamma_t = 9$. From Table V it is seen that when the extracted worst contingencies of the ARO are fixed in the proposed ROUC, the optimal total cost is lower than the case in which the extracted worst contingencies of the proposed ROUC are fixed in the ARO. Thus, it shows that the proposed ROUC has found more critical worst contingencies. Hence, the higher total cost of the proposed ROUC than the ARO in Table I is due to the higher immunization provided by the proposed ROUC against more critical worst contingencies.

C. Comparison With Modified ARO

In order to modify the contingency search capability of the ARO, the proposed LS technique is added to it. In this way, the modified ARO can find the same worst contingencies extracted by the proposed ROUC and thus the same total costs of the proposed ROUC are obtained by the modified ARO in Table I. On the other hand, from the computational time point of view, the proposed solution method is [2.94-3.43] times in case I and [3.03-3.32] times in case II faster than the modified ARO. This difference is related to the higher computational efficiency of the proposed ROUC than the ARO as discussed in the previous section.

TABLE VI
RESULTS OBTAINED FROM THE PROPOSED UNCERTAINTY MODEL, MODEL A, AND MODEL B FOR N-10 CASE WITH $\Gamma_t = 9$

Uncertainty model	Cardinality Budgets	Selected vulnerable lines	Extracted N-10 worst contingencies
A	Ignored	Ignored	13-14/15-16/16-17/11-12 7-8/8-9/6-26/5-6/24-25/1-2
B	Ignored	11-12/12-13/14-15/15-16/ 16-17/32-33/5-6/ 6-7/7-8/10-11/6-26/30-31/31-32/ 2-3/19-20/21-22/23-24/24-25	12-13/14-15/16-17/32-33/6-7/10-11/6-26/30-31/2-3/23-24
Proposed	6	11-12/12-13/14-15/15-16/ 16-17/32-33	12-13/14-15/16-17/32-33
	6	5-6/7-8/10-11/6-26/30-31/ 31-32	7-8/10-11/6-26/30-31
	3	2-3/21-22/24-25	2-3/24-25

D. Comparison With Other Uncertainty Models

The proposed uncertainty model is compared with two other uncertainty models, denoted as model A and model B:

Model A) This model [34] includes conventional uncertainty sets which do not consider the failure probabilities of branches and the spatiotemporal dynamics of windstorm. Model B) This model [4], [17] considers branch failure probabilities, while windstorm spatiotemporal dynamics are not modeled. In other words, this uncertainty model assumes that the entire network is affected by windstorm at the same time with the same speed.

For the sake of a fair comparison, all uncertainty models have been implemented within the ROUC framework. The results obtained from the three uncertainty models are presented in Table VI. This table shows that approach A cannot model uncertainty budgets and vulnerable lines, and approach B cannot model cardinality budgets. In addition, it is seen that the extracted worst contingencies by model A, model B, and the proposed model are different. Uncertainty model A extracts 10 worst contingencies among all 32 lines of the network without considering their failure probabilities and geographical locations. Thus, four non-vulnerable lines are also selected by this uncertainty model (including 13-14,11-12, 8-9 and 1-2 lines) indicated by red color in Table VI. Moreover, approach A has to search among 32 lines to find 10 worst contingencies instead of searching among 15 vulnerable lines as in the proposed model. Therefore, the computation time of the ROUC with uncertainty model A increases to 1193s for $\Gamma_t = 9$ which is significantly higher than the computation time of the ROUC with the proposed uncertainty model, i.e., 544s, for $\Gamma_t = 9$. There are a fewer number of non-vulnerable lines (including two lines 6-7 and 23-24) in the worst contingencies extracted by model B than model A. Although model B considers branch failure probabilities, it does not take into account wind speed variations, chronological order of contingencies, and geographical locations of power branches. Thus, some non-vulnerable lines are selected as vulnerable lines and extracted worst contingencies. In addition, since model B requires searching among all branches of a distribution network to find the vulnerable ones (while the proposed uncertainty model requires searching among smaller zonal sets of branches), the computation time with uncertainty model B is 608s for this test case, which is higher than the 544s computation time of the proposed uncertainty model. Table VI shows that there is no non-vulnerable line in both selected vulnerable lines and extracted worst contingencies by the proposed uncertainty model, as it considers branch failure probabilities and windstorm spatiotemporal dynamics.

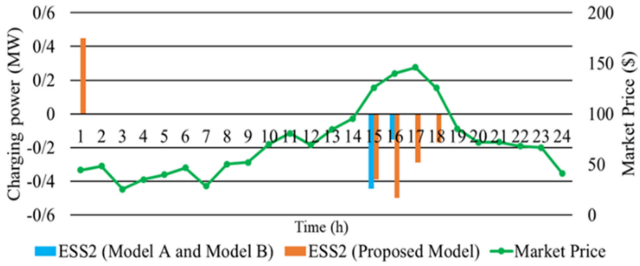

Fig. 3. ESS_2 charging/discharging power obtained by model A, model B, and proposed model for case I with $\Gamma_t = 9$.

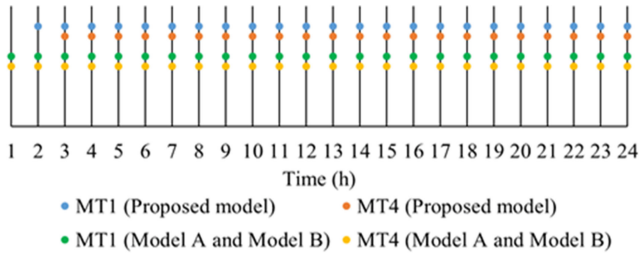

Fig. 4. MT scheduling results obtained by model A, model B, and proposed model for case I with $\Gamma_t = 9$.

In Fig. 3 and Fig. 4, the results obtained from the ROUC with the three uncertainty models are compared. Fig. 3 shows the charging/discharging power of ESS_2 which is disconnected from energy sources due to line 6-26 contingency. Although all three models have selected this contingency, there is an important difference between the decisions made using these models. Since the proposed uncertainty modeling approach models the chronological order of contingencies, it detects that the windstorm reaches zone 2, where ESS_2 is placed, at time t_2. Thus, as shown in Fig. 3, it charges ESS_2 at time t_1 (i.e., before disconnection of ESS_2) as much as possible, while models A and B do not do that since these models cannot consider the chronological order of contingencies and assume that the entire network is affected by the windstorm at the beginning. Hence, ESS_2 discharges more in the proposed model than in models A and B, at hours with the highest market prices, for decreasing the windstorm consequences, as illustrated in Fig. 3. Similarly, Fig. 4 shows that models A and B commit MT1 and MT4 at t1. However, the proposed model considers that the windstorm reaches MT1 and MT4 (in zones 2 and 3, respectively) at t_2 and t_3. Thus, it does not commit MT1 and MT4 before these times to benefit from the more profitable source of energy purchase from the upstream grid, as it has a lower price than the MTs' generation costs. However, when the windstorm reaches zones 2 and 3, the proposed model starts these MTs to support the network since the multiple contingencies cause disconnection of the network from the upstream grid. With these significant

advantages, the proposed uncertainty model leads to a more resilient and more economical solution with a lower computation time compared to the alternative uncertainty models A and B.

VI. Conclusion

This paper presents a new bi-level robust ROUC model for the optimal operation of an active distribution network to enhance its operational resilience against windstorms. The main findings of this paper can be summarized as follows:

1) The proposed zonal wind-speed-specific uncertainty set models the spatiotemporal dynamics of windstorm and the failure probability of branches based on their geographical locations. Therefore, the proposed uncertainty model selects vulnerable branches considering wind speed variations and extracts a practical scenario of worst contingencies.
2) Unlike conventional uncertainty set for contingencies [33] or the uncertainty set based only on failure probabilities [4], [17], the proposed zonal wind-speed-specific uncertainty set can consider the chronological order of contingencies. It has been shown that the proposed uncertainty model leads to a more resilient and more economical ROUC solution in comparison with other uncertainty models.
3) The proposed bi-level ROUC model has higher flexibility and computational efficiency than tri-level ARO. Its reason is that the proposed ROUC model determines the commitment and dispatch variables simultaneously, considering their interactions, while tri-level ARO should solve two large problems iteratively.
4) It has been shown that the proposed ROUC extracts more critical worst contingencies compared to ARO. Thus, the proposed ROUC can provide higher resilience against windstorms than ARO. In addition, the higher effectiveness of the proposed ROUC compared to ARO is illustrated using an out-of-sample analysis.
5) The degree of robustness of the proposed ROUC against uncertain continuous parameters can be controlled using the bounded intervals and the budget of uncertainty. Moreover, the immunization level of the ROUC against windstorm caused contingencies can be controlled using the cardinality budgets. However, higher robustness/immunization levels against uncertain/binary uncertain parameters typically lead to higher operation costs.
6) Unlike the conventional duality-based and KKT-based solution methods, the proposed BCD+LS solution approach can solve robust optimization problems with binary decision variables in the second level. In addition, the proposed BCD+LS solution method can extract the worst-case realization considering both binary and continuous uncertain parameters, as well as their interactions.

Extending the proposed ROUC model to study planning-oriented resilience measures is considered as future work. Placement of distributed energy resources coordinated with effective hardening strategies to increase the infrastructural resilience of distribution networks will be studied next.

References

[1] D. T. Ton and W-T. P. Wang, "A more resilient grid: The U.S. department of energy joins with stakeholders in an R&D plan," *IEEE Power Energy Mag.*, vol. 13, no. 3, pp. 26–34, May/Jun. 2015.

[2] Executive Office of the President, "Economic benefits of increasing electric grid resilience to weather outages," Aug. 2013. [Online]. Available: https://www.energy.gov/sites/prod/files/2013/08/f2/Grid%20Resiliency%20Report_FINAL.pdf

[3] A. Gholami, F. Aminifar, and M. Shahidehpour, "Front lines against the darkness: Enhancing the resilience of the electricity grid through microgrid facilities," *IEEE Electrific. Mag.*, vol. 4, no. 1, pp. 18–24, Mar. 2016.

[4] H. Ma, B. Chen, and Z. Wang, "Resilience enhancement strategy for distribution systems under extreme weather events," *IEEE Trans. Smart Grid*, vol. 9, no. 2, pp. 1442–1451, Mar. 2018.

[5] Z. Li, M. Shahidehpour, F. Aminifar, A. Alabdulwahab, and Y. Al-Turki, "Networked microgrids for enhancing the power system resilience," *Proc. IEEE*, vol. 105, no. 7, pp. 1289–1310, Jul. 2017.

[6] A. Gholami, T. Shekari, M. H. Amirioun, F. Aminifar. and M. H. Amini, "Toward a consensus on the definition and taxonomy of power system resilience," *IEEE Access*, vol. 6, pp. 32035–32053, 2018.

[7] A. Gholami, T. Shekari, and F. Aminifar, "Microgrid scheduling with uncertainty: The quest for resilience," *IEEE Trans. Smart Grid*, vol. 7, no. 6, pp. 2849–2858, Nov. 2016.

[8] Y. Wang, Y. Xu, J. He, and C. C. Liu, "Coordinating multiple sources for service restoration to enhance resilience of distribution systems," *IEEE Trans. Smart Grid*, vol. 10, no. 5, pp. 5781–5793, Sep. 2019.

[9] S. Poudel and A. Dubey, "Critical load restoration using distributed energy resources for resilient power distribution system," *IEEE Trans. Power Syst.*, vol. 34, pp. 52–63, no. 1, Jan. 2019.

[10] Y. Almoghathawi, K. Barker, and L. A. Albert, "Resilience-driven restoration model for interdependent infrastructure networks," *Rel. Eng. Syst. Safety*, vol. 185, pp. 12–23, May 2019.

[11] Y. P. Fang and G. Sansavini, "Optimum post-disruption restoration under uncertainty for enhancing critical infrastructure resilience," *Rel. Eng. Syst. Safety*, vol. 185, pp. 1–11, May 2019.

[12] H. Gao, Y. Chen, and Y. Xu, "Resilience-oriented critical load restoration using microgrids in distribution systems," *IEEE Trans. Smart Grid*, vol. 7, no. 6, pp. 2837–2848, Nov. 2016

[13] C. Chen, J. Wang, F. Qiu, and D. Zhao, "Resilient distribution system by microgrids formation after natural disasters," *IEEE Trans. Smart Grid*, vol. 7, no. 2, pp. 958–966, Mar. 2016.

[14] Y. Li, Z. Li, F. Wen, and M. Shahidehpour, "Minimax-regret robust co-optimization for enhancing the resilience of integrated power distribution and natural gas system," *IEEE Trans. Sustain. Energy*, vol. 11, no. 1, pp. 61–71, Jan. 2020.

[15] D. N. Trakas and N. D. Hatziargyriou, "Optimal distribution system operation for enhancing resilience against wildfires," *IEEE Trans. Power Syst.*, vol. 33, no. 2, pp. 2260–2271, Mar. 2018.

[16] M. Panteli, D. N. Trakas, P. Mancarella, and N. D. Hatziargyriou, "Power systems resilience assessment: Hardening and smart operational enhancement strategies," *Proc. IEEE*, vol. 105, no. 7, pp. 1202–1213, Jul. 2017.

[17] M. H. Amirioun, F. Aminifar, and H. Lesani, "Resilience-oriented proactive management of microgrids against windstorms," *IEEE Trans. Power Syst.*, vol. 33, no. 4, pp. 4275–4284, Jul. 2018.

[18] General Electrics LM6000 series manual. [Online]. Available: https://www.ge.com/power/gas/gas-turbines/lm6000. Accessed on: Jul. 2018.

[19] A. Gholami, T. Shekari, and S. Grijalva, "Proactive management of microgrids for resiliency enhancement: An adaptive robust approach," *IEEE Trans., Sustain. Energy*, vol. 10, no. 1, pp. 470–80, Jan. 2019.

[20] National Oceanic and Atmospheric Administration storm database. [Online]. Available: https:// www.ncdc.noaa.gov/stormevents. Accessed on: Sep. 2018.

[21] W. Yuan, J. Wang, and F. Qiu, "Robust optimization-based resilient distribution network planning against natural disasters," *IEEE Trans. Smart Grid*, vol. 7, no. 6, pp. 2817–2826, Nov. 2016.

[22] A. Shafieezadeh, U. P. Onyewuchi, M. M. Begovic, and R. DesRoches, "Age-dependent fragility models of utility wood poles in power distribution network against extreme wind hazards," *IEEE Trans. Power Del.*, vol. 29, no. 1, pp. 131–139, Feb. 2014.

[23] S. Bjarnadottir, Y. Li, and M. G. Stewart, "Hurricane risk assessment of power distribution poles considering impacts of a changing climate," *J. Infrastruct. Syst.*, vol. 19, pp. 12–24, 2012.

[24] M. Panteli, D. N. Trakas, P. Mancarella and N. D. Hatziargyriou, "Boosting the power grid resilience to extreme weather events using defensive islanding," *IEEE Trans. Smart Grid*, vol. 7, no. 6, pp. 2913–2922, Nov. 2016.

[25] M. Tavakoli Bina and T. Akbari, "Approximated MILP model for AC transmission expansion planning: Global solutions versus local solutions," *IET Gener. Transms. Distrib.*, vol. 10, no. 7, pp. 1563–1569, May 2016.
[26] A. J. Wood, B. F. Wollenberg, and G. B. Sheblé, *Power Generation, Operation, and Control*. 3rd Ed., Hoboken, NJ, USA: Wiley Publication, Nov. 2013.
[27] N. Amjady, *Electric Power Systems: Advanced Forecasting Techniques and Optimal Generation Scheduling*, Boca Raton, FL, USA: CRC Press, 2012, Ch.4.
[28] B. Bagheri and N. Amjady, "Adaptive-robust multi-resolution generation maintenance scheduling with probabilistic reliability constraint," *IET Gener. Transms. Distrb.*, vol. 13, no. 15, pp. 3292–3301, Aug. 2019.
[29] Extended form. [Online]. Available: https://drive.google.com/open?id=1KhPeyUYFwgegp5JfFgtC7Y97_2uL7Bgj. Accessed on: Mar. 2019.
[30] M. E. Baran and F. F. Wu, "Network reconfiguration in distribution systems for loss reduction and load balancing," *IEEE Trans. Power Del.*, vol. 4, no. 2, pp. 1401–1407, Apr. 1989.
[31] GAMS solvers manual. [Online]. Available: https://www.gams.com/latest/docs/S_CPLEX.html. Accessed on: Jan. 2018.
[32] N. Amjady, S. Dehghan, A. Attarha, and A. Conejo, "Adaptive robust network-constrained AC unit commitment," *IEEE Trans. Power Syst.*, vol. 32, no. 1, pp. 672–683, Jan. 2017.
[33] S. Dehghan, N. Amjady, and A. J. Conejo, "Reliability-constrained robust power system expansion planning," *IEEE Trans. Power Syst.*, vol. 31, no. 3, pp. 2383–2392, May 2016.
[34] J. M. Arroyo, "Bi-level programming applied to power system vulnerability analysis under multiple contingencies," *IET Gener. Transms. Distrib.*, vol. 4, no. 2, pp. 178–190, Feb. 2010.